Eur. Phys. J. E **11**, 21–28 (2003)
DOI 10.1140/epje/i2002-10125-x

THE EUROPEAN PHYSICAL JOURNAL E

Lateral and transverse diffusion in two-component bilayer membranes

A. Imparato[a], J.C. Shillcock[b], and R. Lipowsky[c]

Max-Planck-Institut für Kolloid- und Grenzflächenforschung, Abteilung Theorie, D-14424 Potsdam, Germany

Received 6 December 2002 and Received in final form 26 March 2003 /
Published online: 27 May 2003 –

Abstract. We study the lateral and transverse diffusion of amphiphiles in two-component bilayer membranes, using a coarse-grained model for amphiphilic molecules and combined Monte Carlo-Molecular Dynamics simulations. Membrane structural properties, such as the mean thickness, are also measured. The dependence of such properties on membrane composition, inter-molecular interactions, and amphiphile stiffness is determined. In particular, we show that addition of shorter amphiphiles drives the model membrane towards a more fluid state, with increased amphiphile lateral diffusion rates. These results can be understood in the framework of a simple free-volume model. Furthermore, we observe an increase in the trans-membrane diffusion when the interaction energy of amphiphiles with their neighboring molecules is decreased.

PACS. 82.70.-y Disperse systems; complex fluids – 61.20.Ja Computer simulation of liquid structure

1 Introduction

Supramolecular aggregates of amphiphilic molecules are essentially characterized by two length scales: on the one hand, the molecules can be viewed as semi-flexible rods, with a length of the order of 1-2 nm; on the other hand, they often form a bilayer membrane which has a lateral extension that can reach several micrometers. This is reflected in two different approaches used to model such systems: in the first approach, the membranes are treated as smooth elastic surfaces in such a way that only the properties depending on the largest length scale are taken into account [1]; alternatively, on the molecular length scale, one is forced to use a small number of molecules in Molecular Dynamics simulations, because of the large amount of computation time required [2–6]. In this case, coarse-grained models for the amphiphile-water solution, have been proposed in order to reduce the computation time. These models keep some of the molecular features of the water and amphiphile and have been shown to reproduce many general and local properties of the water-bilayer system, such as self-assembly of bilayers in water with typical lateral density profiles [7,8], or the fluctuation spectrum of a membrane [9].

These models were characterized by a single type of amphiphile, in contrast to natural membranes which are multi-component systems and contain many different types of lipids and proteins. In the present article, we extend the coarse-grained model introduced in [7] and consider two types of model amphiphiles, which differ mainly in their chain lengths, and study how the bilayer composition and the inter-molecular interactions influence dynamic properties such as lateral and transverse diffusion of the lipids within the bilayer. The study of such properties can provide useful information on transport phenomena in biological and biomimetic membranes such as Black Lipid Membranes (BLM) [10]. In particular, we observe an increase of the amphiphile's lateral diffusion as the fraction of shorter amphiphiles is increased and we propose a simple free-volume model to explain this result.

Our article is organized as follows. In Section 2, we describe the details of our membrane models and of our simulation method. We then present the results of our numerical simulations, first for the lateral diffusion in Section 3.1 and then for the transverse diffusion in Section 3.2.

2 Modelling on the supramolecular scale

2.1 Particles and interaction potentials

We use the same coarse-grained model for both the solvent and the amphiphilic molecules that was used in [7]: the water particle (W), the amphiphile head-group (H) and several CH_2 groups of an amphiphile hydrocarbon chain (C) are represented by single particles. We extend that

[a] e-mail: imparato@mpikg-golm.mpg.de
[b] e-mail: shillcock@mpikg-golm.mpg.de
[c] e-mail: lipowsky@mpikg-golm.mpg.de

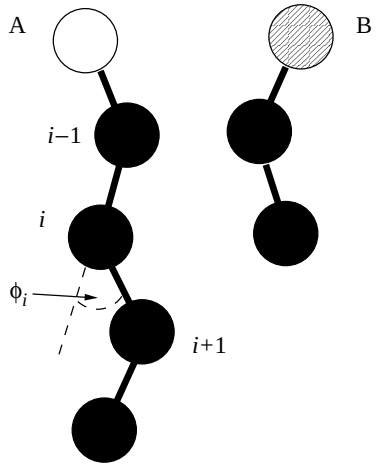

Fig. 1. Example of the two amphiphiles A and B.

Table 1. Interaction potentials between the 4 different particles of the model.

$U_{\alpha\beta}$	W	H_A	H_B	C
W	U_{LJ}	U_{LJ}	U_{LJ}	U_{SC}
H_A	U_{LJ}	U_{LJ}	U_{LJ}	U_{SC}
H_B	U_{LJ}	U_{LJ}	U_{LJ}	U_{SC}
C	U_{SC}	U_{SC}	U_{SC}	U_{LJ}

model by introducing two kinds of amphiphiles, a longer one (A) and a shorter one (B), as shown in Figure 1. In our model, the two amphiphiles differ in their length, *i.e.* the number of C particles, and in the interaction of their heads with the other particles; hence, in the following, we distinguish between the two head particles H_A and H_B, while the C particles have the same properties for both types of amphiphilic molecules. The hydrophobic interaction of C with H and W particles is modelled by the repulsive soft-core (SC) potential

$$U_{SC}(r_{ij}) = 4\epsilon_{\alpha\beta}\left(\frac{\sigma'_{\alpha\beta}}{r_{ij}}\right)^9 , \qquad (1)$$

while all the other attractive interactions, W-W, W-H, H-H, C-C, are modelled by the Lennard-Jones (LJ) potential

$$U_{LJ}(r_{ij}) = 4\epsilon_{\alpha\beta}\left[\left(\frac{\sigma_{\alpha\beta}}{r_{ij}}\right)^{12} - \left(\frac{\sigma_{\alpha\beta}}{r_{ij}}\right)^{6}\right] , \qquad (2)$$

where $\alpha, \beta \epsilon \{W, H_A, H_B, C\}$. The interactions between the four kinds of particle are summarized, using a matrix notation, in Table 1. We use a cutoff radius $\sigma_c = 2.5\sigma_{\alpha\beta}$, for the LJ interaction, and a cutoff radius $\sigma'_c = 2.5\sigma'_{\alpha\beta}$ for the SC interaction, *i.e.*, these interactions vanish for $r > \sigma_c$ and $r > \sigma'_c$, respectively.

Our model contains two other types of force potential. Adjacent particles in one amphiphilic molecule are connected via the harmonic potential

$$U_2(r_{i,i+1}) = k_2\left(r_{i,i+1} - \sigma\right)^2 , \qquad (3)$$

where i and $i+1$ indicate two successive particles along the chain. To model the effects of hydrocarbon chain stiffness, all particles within a single amphiphile molecule interact also via the three-body bending potential

$$U_3(\mathbf{r}_{i-1,i}, \mathbf{r}_{i,i+1}) = k_3\left(1 - \frac{\mathbf{r}_{i-1,i}\cdot\mathbf{r}_{i,i+1}}{r_{i-1,i}\, r_{i,i+1}}\right) = k_3(1-\cos\phi_i) , \qquad (4)$$

where $\mathbf{r}_{i,i+1} = \mathbf{r}_{i+1} - \mathbf{r}_i$, see Figure 1.

2.2 Simulation method

Our system contains $N = N_W + N_{H_A} + N_{H_B} + N_C$ particles, where N_W, N_{H_A}, N_{H_B} and N_C are the number of W, H_A, H_B and of C particles, respectively. We use a cuboidal simulation box, with periodic boundary conditions in all three directions. The volume of the box is given by $L_\parallel^2$, $L_\perp$, where $L_\parallel$ and $L_\perp$ are the lengths of the box sides parallel and perpendicular to the bilayer membrane, respectively. The overall particle density is

$$\rho = N/(L_\parallel^2 L_\perp) , \qquad (5)$$

and the amphiphile concentration is defined by

$$c = \frac{N_{H_A} + N_{H_B} + N_C}{N} . \qquad (6)$$

In order to simulate this system, we use a combined Monte Carlo (MC)-Molecular Dynamics (MD) code. Through the MC algorithm, we let the system evolve towards configurations of minimal potential energy at a given temperature. The configurations obtained after about $500\times N$ MC steps are used as starting configurations for the MD part of the simulation: the equations of motion for the model system described above are integrated using a *velocity* Verlet algorithm which is very efficient from a computational point of view [11]. We rescaled the particle velocities, at every time step in order to keep the temperature constant, as used before in reference [7]. While such rescaling is not essential, and is used only to reduce the temperature fluctuations, we have checked that results obtained without the rescaling are statistically equivalent (data not shown).

In order to save computation time, we always use preassembled planar bilayers, as starting configurations, since the capability of the model to evolve towards a bilayer configuration, starting from a random configuration of the particles, has already been demonstrated in [7].

2.3 Model parameters

As far as the MC simulations are concerned, our model is uniquely defined in terms of the interaction parameters introduced in Section 2.1 above. In order to reduce the number of model parameters, all interaction ranges, $\sigma_{\alpha\beta}$, of the LJ potential, are taken to be equal to σ, and all interaction ranges, $\sigma'_{\alpha\beta}$, of the repulsive SC potential,

are taken to be $\sigma_{\alpha\beta} = 1.05\sigma$ as in [7]: with this choice, the hard-core repulsion of the SC potential is approximately as strong as the repulsive part of the LJ potential. Likewise, all energy parameters, $\epsilon_{\alpha\beta}$, are taken to have the same value ϵ unless one of the interacting particles is a head-group particle H_B of a short-chain B-amphiphile, as discussed below. The reason for this choice is that we wanted to study the behavior of a second type of amphiphile that is smaller than the major amphiphile and has distinct head-group properties; examples of such system are provided by cholesterol or fatty acids in a lipid bilayer.

For the strength of the harmonic bond potential (3) and of the three-body bending potentials (4), we use the constant parameter values $k_2 = 5000\epsilon/\sigma^2$ and $k_3 = 2\epsilon$, as in previous work [7], in all the simulations here described, except for the simulations described in Section 3.2 where the values $k_3 = 2\epsilon$ and $k_3 = 20\epsilon$ are used for the shorter B-amphiphile.

For the MD simulations, our model involves the following additional parameters: i) the masses m_i of the different particles which enter the equations of motions, and ii) the time step Δt used to discretize these equations. For simplicity, we choose all particles to have the same mass $m_i = m$. Using this mass parameter, we obtain the basic time scale $t_{sc} = \sqrt{m\sigma^2/\epsilon}$. For the LJ interaction length σ and particle mass m, we take the values already used in [7]: $\sigma = 1/3$ nm which is of the same order as the LJ lengths of interactions for pairs of particles, in which each particle can represent a CH_2 group or a CH_3 group or a water molecule, as discussed in [12], and $m = (0.036/N_{Av})$ kg, which is the mean value between the mass of a water molecule and the mass of four CH_2 groups (N_{Av} is the Avogadro number). As mentioned, the energy $\epsilon_{\alpha\beta}$ that appears in (1) and (2) is varied only for the interaction of pairs in which one of the particles is a H_B, for all the other interactions the energy is fixed: $\epsilon_{\alpha\beta} = \epsilon$, if $\alpha, \beta \neq$ B. We used $\epsilon = (2/N_{Av})$ kJ which is the same value as in [7]. This value is bigger than the LJ energies for pairs of CH_2 groups and/or water molecules reported in [12], but it takes into account that in our model one C particle corresponds to three or four CH_2 groups. Using this value of ϵ one obtains the time scale $t_{sc} = \sqrt{m\sigma^2/\epsilon} = 1.4$ ps. In our MD simulations, the integration time step Δt was set to $\Delta t = t_{sc}/2000 = 0.7$ fs. All the simulations were performed at the temperature $k_B T = 1.35\epsilon$, which corresponds to a temperature of 325 K or 50 °C.

In the following, we will use the parameters σ, ϵ, and m as the basic length, energy, and mass scales. Using these scales, we will define reduced and dimensionless quantities which are indicated by a bar. Thus, the reduced particle density and diffusion coefficient are given by $\bar{\rho} = \rho\sigma^3$ and $\bar{D} = D\sqrt{m/\sigma^2\epsilon}$, respectively. There is one exception to this rule: the reduced time is taken to be $\bar{t} = t/\Delta t$ (rather than t/t_{sc}).

We varied the ratio of A to B keeping constant the dimensionless particle density (solvent + amphiphiles) $\bar{\rho} = 1/3$, the amphiphile concentration $c \simeq 0.44$ (see Eq. (6)), and the simulation box sizes $\bar{L}_\parallel = 12.24$, $\bar{L}_\perp = 14.415$.

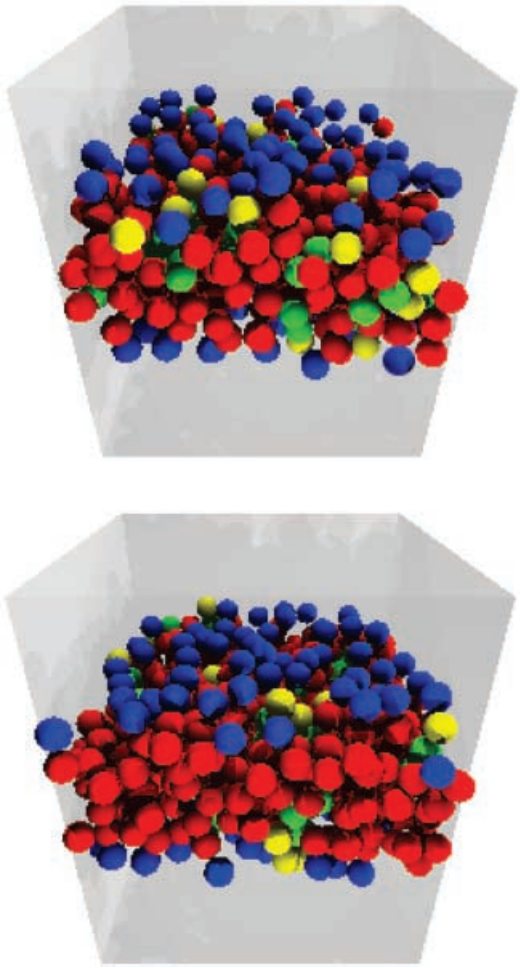

Fig. 2. Two snapshots, taken at different instants of an MD simulation, of a bilayer with $N_A = 113$ longer-tailed amphiphiles, $N_B = 25$ shorter-tailed amphiphiles, $N_W = 800$ solvent particles. The blue, yellow, red, green beads represent the H_A, H_B, C of A-amphiphile, C of B-amphiphile particles, respectively. We use different colors for the C particles of the two amphiphiles only to distinguish them in the pictures. The solvent particles are not shown.

These values were shown in [7] to be the most suitable in order to obtain a well-behaved bilayer. In a typical pure A-amphiphile bilayer, we use $N_A = 128$, $N_W = 800$. In Figure 2 two snapshots of a bilayer with $N_A = 113$, $N_B = 25$, at different instants of an MD simulation, are shown.

3 Diffusion of amphiphiles

In a bilayer membrane, the motion of amphiphiles is largely restricted to one of the two monolayers, with rare *trans-membrane* diffusion or flip-flops. One has therefore to distinguish between two motions of the amphiphiles: a lateral and a transverse diffusive motion, characterized by two different diffusion coefficients $D_\parallel$ and $D_\perp$. At the beginning of each numerical experiment, we zero the center-of-mass velocity of all the particles in the system, in order

to avoid overall drift of the membrane along the direction perpendicular to its plane. We have measured the diffusion coefficients of the W particles and of the A-amphiphiles by fitting their mean-square displacement (MSD) at large times, according to the asymptotic relation

$$D_\alpha = \lim_{t\to\infty} D_\alpha(t) = \lim_{t\to\infty} \frac{\sum_k \left[\mathbf{r}_k(t) - \mathbf{r}_k(0)\right]^2}{6N_\alpha t}, \qquad (7)$$

where $\alpha = \mathrm{W}, \mathrm{A}$. Although the diffusion coefficient may, in general, show a non-linear time dependence, we have used the linear relation (7) to measure it at large times, where we verified, using a log-log fit, that the MSD grows linearly with time. In (7), if $\alpha = \mathrm{W}$, $\mathbf{r}_k$ is the position vector of the k-th water particle and N_W is the number of W particles in the system, while if $\alpha = \mathrm{A}$, $\mathbf{r}_k$ is the center-of-mass position vector of the k-th A-amphiphile and N_A is the number of A-amphiphile considered. The diffusion coefficient $D_\parallel$, for lateral diffusion parallel to the bilayer, is then defined via

$$D_{\alpha\parallel} = \lim_{t\to\infty} \frac{\sum_k \left[\mathbf{r}_{k\parallel}(t) - \mathbf{r}_{k\parallel}(0)\right]^2}{6N_\alpha t}, \qquad (8)$$

where $\mathbf{r}_{k\parallel}$ is the projection of the position vector of the k-th water particle/amphiphile into the plane of the membrane. The diffusion coefficient $D_\perp$ for the transverse diffusion is given by

$$D_{\alpha\perp} = D_\alpha - D_{\alpha\parallel}\,. \qquad (9)$$

The parallel and perpendicular directions are taken along the box axes; because the bilayer shape fluctuations are small, its overall normal direction is always very close to the z-axis, see Figure 2. For the amphiphiles, the occurrence of flip-flops was observed in the following way. Starting from a given bilayer configuration, the amphiphiles belonging to the upper and to the lower monolayer were labelled with two different labels. Every time an amphiphile enters the opposite monolayer, its label is changed and one flip-flop is counted. Figure 3 shows that the motion of the A-amphiphiles is confined to the bilayer surfaces, indeed $D_{\mathrm{A}\parallel} \simeq D_\mathrm{A}$, and no flip-flops were observed during each simulation which lasted $2 \cdot 10^6$ MD time steps. In the same figure, the diffusion coefficient for the water particles is also shown. Note that $D_\mathrm{W} \simeq D_{\mathrm{W}\parallel}$, for large $\bar{t}$, which shows that the bilayer is impermeable to the W particles, since these particles are rather large in our model and have the same size as the H and C particles of the amphiphiles. In order to study the permeability of the bilayer membrane to water, one should use W particles, which are small compared to the H and C particles. Note that the reduced diffusion coefficient $\bar{D}_\mathrm{A}$ is of the order of 10^{-2}, which implies that the dimensionful coefficient $D_\mathrm{A} = \bar{D}_\mathrm{A}\sqrt{\sigma^2\epsilon/m}$ is of the order of 10^{-5} cm^2/s, since our parameter choice leads to $\sqrt{\sigma^2\epsilon/m} \simeq 0.8 \times 10^{-3}\,\mathrm{cm}^2/\mathrm{s}$.

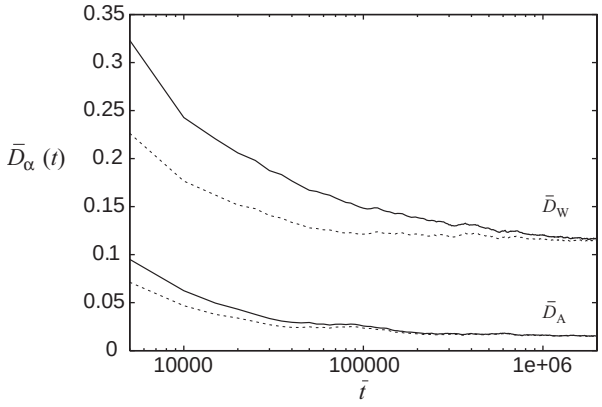

Fig. 3. Reduced diffusion coefficient $\bar{D}_\alpha(t)$, as a function of the number of MD steps $\bar{t}$, for W particles and A-amphiphiles, in a one-component A bilayer. The two dotted lines correspond to the lateral diffusion coefficient defined in (8), for both W particles and A-amphiphiles.

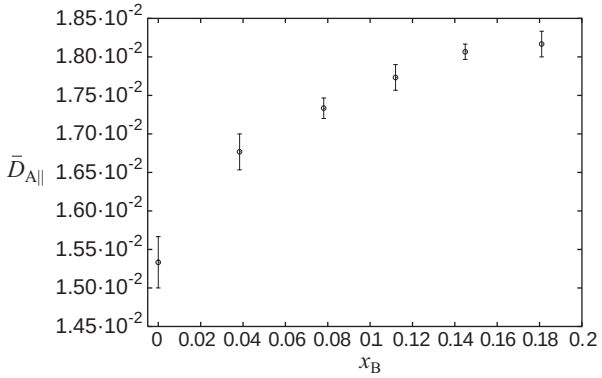

Fig. 4. Reduced diffusion coefficient $\bar{D}_\parallel$ for the A-amphiphiles, as function of the B-amphiphile fraction x_B.

3.1 Lateral diffusion of A-amphiphiles

We measured the diffusion coefficient of A-amphiphiles as a function of the mole fraction

$$x_\mathrm{B} \equiv \frac{N_\mathrm{B}}{N_\mathrm{A} + N_\mathrm{B}} \qquad (10)$$

of B-amphiphiles, where N_A and N_B are the number of A- and B-amphiphiles, respectively. These experiments were performed taking $\epsilon_{\alpha,\mathrm{B}} = \epsilon/4$ for $\alpha = \mathrm{W}$, $\mathrm{H_A}$, $\mathrm{H_B}$, C. For each value of x_B, the system was equilibrated with 10^6 MC and $2{\cdot}10^6$ MD steps, and then five successive runs of $2{\cdot}10^6$ MD steps were performed, where each run started with the final configuration of the previous one. This corresponds to a total simulation length $5 \times 2 \cdot 10^6 \times 0.7\,\mathrm{fs} = 7\,\mathrm{ns}$. The diffusion coefficient was determined for each of the five runs and then averaged.

As shown in Figure 4, increasing the fraction x_B of short B-chain amphiphiles, increases the diffusion of A-amphiphiles in the monolayers. For constant overall density ρ and amphiphile concentration c, an increase of x_B leads to an increase of the total number of amphiphiles and to a decrease of the total number of tail particles,

Table 2. Number of amphiphile ($N_{\rm amph} = N_{\rm A} + N_{\rm B}$) and C particles for the different B-amphiphile concentration used in the numerical experiments for the determination of the diffusion coefficient of the A-amphiphile.

$x_{\rm B}$	$N_{\rm amph}$	$N_{\rm C}$
0	128	512
0.0384	130	510
0.07576	132	508
0.112	134	506
0.14706	136	504
0.181	138	502

as shown in Table 2. In addition, the bilayer thickness, which we define to be the average distance between the two monolayers, is found to be $d \simeq 5.6\sigma$ and to change by less than 2% for the range of $x_{\rm B}$ shown in Figure 4. Thus, the increase of lateral diffusion should arise from the decrease of the density in the hydrophobic part of the bilayer which is composed of C particles, *i.e.*, from the fact that the tails of the A-amphiphiles have a greater mean free-volume, as $x_{\rm B}$ is increased[1].

We find that the bilayer is unstable to large shape fluctuations and amphiphile protrusions, if a fraction of B-amphiphiles greater than the maximum value here considered ($x_{\rm B} \simeq 0.2$) is added, this is the reason why we do not consider bilayers with a greater amount of shorter amphiphiles in the present work.

According to the free-volume theory of Cohen and Turnbull [13,14], the diffusion of a particle through a liquid of the same molecular size occurs via density fluctuations in the liquid, which lead to the formation of a free volume next to the particle, provided this free volume exceeds a certain critical value. Ferry [15] extended these arguments to diffusion in polymer solutions at any temperature. Within these theories, one derives an exponential dependence for the diffusion coefficient D on the mean free volume $v_{\rm f}$ of a diffusing particle. This free volume is decomposed as $v_{\rm f} = v - v_{\rm f}^*$, where v is the mean particle volume in the fluid and $v_{\rm f}^*$ is a critical free volume. The diffusion coefficient is given by

$$D(v) = D_0 \exp\left[-\frac{\gamma v_{\rm f}^*}{v_{\rm f}}\right] = D_0 \exp\left[-\frac{\gamma v_{\rm f}^*}{v - v_{\rm f}^*}\right], \qquad (11)$$

where γ is a geometric factor and D_0 is the limiting diffusion rate for free volumes much greater than the critical

[1] The surface tension of the pure long-chain amphiphilic bilayer, measured with the method described in [7], is small but positive. We view our system as a model of a black lipid membrane stretched across a hole in a teflon plate, and such systems typically have a small positive surface tension. We verified that even if the total number of amphiphiles increases as $x_{\rm B}$ increases (see Tab. 2), the surface tension does not change much more than the statistical errors, in the range of $x_{\rm B}$ here considered. This can be explained by noting that the B-head particles have a smaller interaction energy $\epsilon_{\rm B}$ than the A-head particles, and so their contribution to the surface tension is smaller than the contribution of the A-head particles.

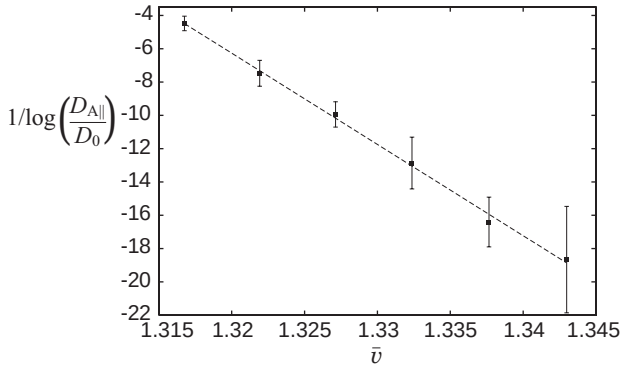

Fig. 5. Plot of the rescaled lateral diffusion coefficient $D_{\rm A\,\parallel}$ as a function of the dimensionless mean volume $\bar{v}$ of the C particles. The line is our least-squares fit to the data.

one. We fit our data for $D_{\rm A\,\parallel}$ to the exponential form as in (11), where γ and $v_{\rm f}^*$ are two fit parameters. For v, we use the value $v = \mathcal{V}/N_{\rm C}$, where $\mathcal{V}$ is the volume of the hydrophobic region of the membrane and $N_{\rm C}$ is the total number of chain particles, see Table 2. We estimate D_0 independently by taking the saturation values for $D_{\rm A\,\parallel}$ as obtained by extrapolation of the data in Figure 4 for large $x_{\rm B}$. The data for the lateral diffusion as a function of the dimensionless mean volume $\bar{v} = v/\sigma^3$ are shown in Figure 5.

From the fit, we obtain $v_{\rm f}^* = (1.31 \pm 0.07)\sigma^3$, which is about twice the value of the close-packing specific volume of hard spheres as given by $v_{\rm HS} = \frac{\sqrt{2}}{2}\sigma^3 \simeq 0.707\sigma^3$ [16]: this is the typical size of a void which has to be formed in the bilayer in order for a diffusive process to take place. This result supports our assumption that the lateral diffusion in our model bilayer is driven by free-volume fluctuations. Indeed, considering the C particles as hard spheres, the substitution of A- by B-amphiphiles, leads to the formation of voids of size $v_{\rm f}^*$ in the membrane hydrophobic region, since the B-amphiphiles have two C particles less than the A-amphiphiles. This also indicates that the increase of the number of amphiphiles and, thus, of the head-groups, has a relatively small effect on the diffusion coefficient (see Tab. 2). From the fit we also obtain the value for the prefactor γ, which is $\gamma = (1.40 \pm 0.03) \cdot 10^{-3}$. This indicates a sharp increase in the diffusion process of the amphiphiles in the membrane, as soon as the mean volume v is greater than the critical value $v_{\rm f}^*$.

It is worth noting that in other theoretical and experimental works [17–19] on lipid diffusion in fluid phases, the functional dependence of the lateral diffusion coefficient on the specific area per lipid was found to follow an exponential relationship as in (11). These relationships are, in fact, equivalent to (11) since the specific area per lipid was obtained by dividing the bilayer specific volume by its thickness.

3.2 Flip-flop

The trans-membrane diffusion or flip-flop of amphiphiles, is governed by a different diffusion mechanism. The longer

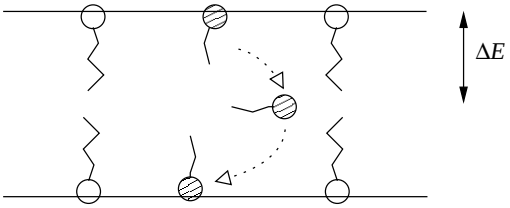

Fig. 6. Schematic flip-flop of a B-amphiphile.

Table 3. Reduced energy parameter $\bar{\epsilon}_{\alpha\beta} = \epsilon_{\alpha\beta}/\epsilon$ for the pair potentials in the simulations on the flip-flop rate of B-amphiphiles.

$\bar{\epsilon}_{\alpha\beta}$	W	H_A	H_B	C
W	1	1	$\bar{\epsilon}_B$	1
H_A	1	1	$\bar{\epsilon}_B$	1
H_B	$\bar{\epsilon}_B$	$\bar{\epsilon}_B$	$\bar{\epsilon}_B$	$\bar{\epsilon}_B$
C	1	1	$\bar{\epsilon}_B$	1

A-amphiphiles exhibit very rare flip-flop events; in fact, we could not observe any flip-flops of these amphiphiles in $2 \cdot 10^6$ MD steps. Switching our attention to the flip-flops of the shorter B-amphiphiles, we expect their shorter tails to facilitate this process. Figure 6 shows a cartoon of the flip-flop of a B-amphiphile.

In the following, the interaction energy between the B-amphiphile's head particle with all the other particle species is taken to be ϵ_B, which will, in general, differ from the basic interaction parameter ϵ. The complete set of energy parameters $\epsilon_{\alpha\beta}$ for the different types of pair potentials is displayed in Table 3. We will now describe how the flip-flop rate of the B-amphiphiles depends on the reduced interaction parameter $\bar{\epsilon}_B = \epsilon_B/\epsilon$. All data discussed in this subsection have been obtained for fixed mole fraction of the B-amphiphiles: $x_B \simeq 0.08$.

We measure the flip-flop rate as a function of $\bar{\epsilon}_B$ for two different values of the chain stiffness of the B-amphiphiles, $k_{3,B} = 2\epsilon$ and $k_{3,B} = 20\epsilon$, whereas the chain stiffness of the A-amphiphiles is kept constant and given by $k_{3,A} = 2\epsilon$. For each value of $\bar{\epsilon}_B$ and $k_{3,B}$, the system was equilibrated with 10^6 MC and $2 \cdot 10^6$ MD steps, and then five successive runs of 10^6 MD steps were performed. The flip-flop rate was determined for each of the five runs and then averaged.

The results of these simulations are shown in Figure 7. For $\bar{\epsilon}_B = 1$, no flip-flops of the B-amphiphiles are observed, in simulation times of $2 \cdot 10^6$ steps, similarly to the A-amphiphiles. Inspection of Figure 7 shows that the flip-flop rate depends exponentially on the interaction energy $\bar{\epsilon}_B$, with two different prefactors for the two different values of $k_{3,B}$. It is evident that stiffer B-amphiphiles cross the bilayer more slowly, and this is probably due to the greater time they need to rotate their tails which behave like rigid rods in the hydrophobic membrane region. It is natural to assume that the flip-flop process represents an activated process with an activation barrier which is primarily determined by the translocation of the hydrophilic

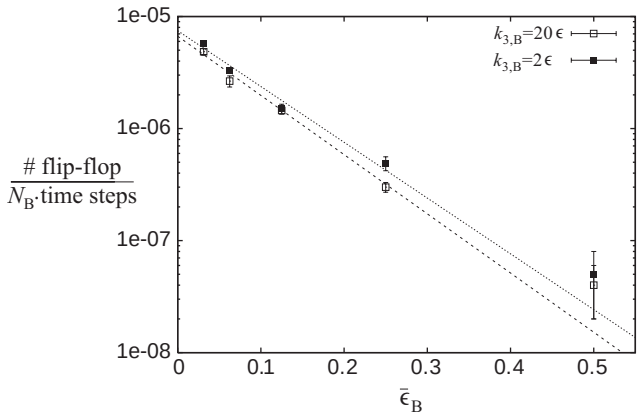

Fig. 7. Flip-flop rate of the B-amphiphiles as a function of the reduced energy $\bar{\epsilon}_B$, for two values of the chain stiffness $k_{3,B}$. The lines are the least-squares fits to the data.

H_B particle through the hydrophobic membrane region. Therefore the characteristic time t_{FF} for a flip-flop to occur should follow an Arrhenius-like law as given by

$$t_{FF} \sim \exp\left[\frac{\Delta E}{k_B T}\right], \tag{12}$$

where ΔE is the energy barrier that a amphiphile has to overcome in order to cross the hydrophobic region of the bilayer (see Fig. 6), and k_B is the Boltzmann constant.

From the data shown in Figure 7, it is clear that the energy barrier which appears on the right side of (12), is proportional to the interaction parameter ϵ_B, *i.e.* the flip-flop rate is strongly affected by the interaction of the B-amphiphile's head with its neighbors. A least-squares fit to the data in Figure 7 leads to $\Delta E \simeq b\epsilon_B$, with $b = 11$ and $b = 12$ for $k_{3,B} = 2\epsilon$ and 20ϵ, respectively.

In order to obtain an independent estimate for ΔE, we use a simple mean-field calculation to obtain the energies of the H_B particles in the two configurations shown in Figure 6: on the surface of one of the two monolayers and in the middle of the bilayer. We assume that the bilayer plane is essentially flat. Although the actual energy of an amphiphile performing a flip-flop contains several contributions, we assume that an H_B particle at the interface between the hydrophobic and hydrophilic bulk has just two contributions to its potential energy: one comes from the LJ interaction with the other hydrophilic particles, the other comes from the SC interaction with the C particles. We also assume that $\langle U_2 \rangle = 0$, since we verified that $\langle l_i \rangle = \sigma$, where $l_i = |r_i - r_{i+1}|$ is the length of the i-th bond in a chain, and $\sqrt{\langle \Delta l_i^2 \rangle}/\langle l_i \rangle \simeq 10^{-3}$ for each i (data not shown).

With these assumptions, the energy of a H_B particle at the interface is given by

$$E_1 \equiv \rho_W I_{LJ} + \rho_C I_{SC}\,, \tag{13}$$

with

$$I_{LJ} \equiv \int_0^{2\pi} \mathrm{d}\varphi \int_0^{\pi/2} \sin(\theta)\,\mathrm{d}\theta \int_\sigma^{\sigma_c} r^2 \mathrm{d}r\, U_{LJ}(r)\,, \tag{14}$$

$$I_{\rm SC} \equiv \int_0^{2\pi} {\rm d}\varphi \int_{\pi/2}^{\pi} \sin(\theta)\,{\rm d}\theta \int_{\sigma}^{\sigma_{\rm c}} r^2 {\rm d}r\, U_{\rm SC}(r)\,, \qquad (15)$$

where the densities $\rho_{\rm W}$ and $\rho_{\rm C}$ are the mean water density and the mean chain particle density, respectively, which we assume to be independent of the inter-particle distance.

In the middle plane of the bilayer, on the other hand, the H_B particle is completely surrounded by C particles and the energy in this configuration is

$$E_2 = 2\rho_{\rm C} I_{\rm SC}\,. \qquad (16)$$

In this way we find the estimate

$$\Delta E_{\rm MF} = E_2 - E_1 \simeq 7.8\epsilon_{\rm B}\,. \qquad (17)$$

This should be compared with the previously mentioned fits to the data of Figure 7 which lead to $\Delta E = 11\epsilon_{\rm B}$ and $\Delta E = 12\epsilon_{\rm B}$ for $k_{3,\rm B} = 2\epsilon$ and $k_{3,\rm B} = 20\epsilon$, respectively, in reasonable agreement with the rough estimate (17). Hence, the assumption that a flip-flop is an activated process, is supported by our results, and the main contribution to the energy barrier is the interaction energy of the amphiphile head with its neighbor particles. Furthermore, our results indicate that the characteristic time $t_{\rm FF}$ depends only weakly on the chain stiffness of the amphiphiles.

4 Conclusion

We have studied a simple model for a two-component bilayer immersed in water which, in spite of its simplicity, exhibits several non-trivial features of amphiphile diffusion in lipid bilayers.

The lateral diffusion of the long-chain A-amphiphiles was found to increase with increasing mole fraction of the short-chain B-amphiphiles. This can be understood in terms of a free-volume model for the diffusive process since this volume increases by adding shorter amphiphiles in the system. While phospholipid-cholesterol mixtures may have complex head-solvent and head-head interactions, which we have ignored, our results on lateral diffusion are consistent with experiments of Almeida *et al.* [18], who studied lateral diffusion of phospholipids in phospholipid/cholesterol binary multibilayers, and found that the diffusion rate increases with the specific volume per phospholipid. They also found that in the temperature range from the melting temperature of the phospholipids, up to 30 °C, the specific volume per phospholipid, and hence the diffusion coefficient, increase with increasing cholesterol mole fraction. Our results on lateral diffusion are also consistent with those of Polson *et al.* [20], who studied lateral diffusion in lipid-sterol bilayers using MC simulations of a two-dimensional model. The authors found that, in the low-temperature range, the diffusion coefficient of the lipid chains increases as the mole fraction of the sterol (cholesterol or lanesterol) is increased.

We also showed that flip-flops of the short-chain B-amphiphile are accessible to our simulations, provided we reduce the interaction strength $\bar{\epsilon}_{\rm B}$ of the head-group particles H_B. We determined the functional dependence of the flip-flop rate on the interaction parameter $\bar{\epsilon}_{\rm B}$ which was found to be well fitted by an exponential. This shows that flip-flops are activated processes. The corresponding activation barrier was estimated from a simple mean-field calculation. The amphiphile's internal structure (as represented by the chain stiffness) does not appear to have a strong influence on this process. This agrees with some experimental results obtained for the flip-flop of fatty acids across phospholipid vesicles [21] and across human red cells [22]. In those experiments, it was found that the fatty acids diffuse spontaneously across bilayers, and protein-based mechanisms are not required for flip-flops to take place.

Our model succeeds in describing, at least qualitatively, several characteristics of two-component bilayers. It can be further extended to simulate multi-component bilayers, such as lipid-protein mixtures, and to study the dynamic processes in such systems.

Glossary: List of symbols used in the text

$\sigma_{\alpha\beta}$	Range of Lennard-Jones potential between particles of type α and β;
$\sigma'_{\alpha\beta}$	Range of soft-core potential;
$\epsilon_{\alpha\beta}$	Lennard-Jones and soft-core interaction energy;
$\mathbf{r}_{ij}$	Distance vector between the i-th and the j-th particle;
m	Particle mass;
$t_{\rm sc}$	Basic time unit;
Δt	Molecular Dynamics integration time step;
ρ	Overall particle density;
c	Amphiphile concentration;
D_α	Diffusion coefficient of α-amphiphile;
$D_{\alpha\parallel}$	Diffusion coefficient of α-amphiphile in the plane parallel to the bilayer;
v	Mean volume per particle of the hydrophobic region of the bilayer;
$v_{\rm f}$	Mean free volume per particle;
$v_{\rm f}^*$	Critical free volume.

References

1. R. Lipowsky, E. Sackmann (Editors), *Structure and Dynamics of Membranes*, *Handbook of Biological Physics*, Vol. **1** (Elsevier, Amsterdam, 1995).
2. F. Zhou, K. Schulten, J. Phys. Chem. **99**, 2194 (1995).
3. K. Tu, D.J. Tobias, M.L. Klein, Biophys. J. **69**, 2558 (1995).
4. K. Tu, M.L. Klein, D.J. Tobias, Biophys. J. **75**, 2147 (1998).
5. A.M. Smondyrev, M.L. Berkowitz, J. Chem. Phys. **110**, 3981 (1999).
6. A.M. Smondyrev, M.L. Berkowitz, Biophys. J. **77**, 2075 (1999).
7. R. Goetz, R. Lipowsky, J. Chem. Phys. **108**, 7397 (1998).

8. J.C. Shelley, M.Y. Shelley, R.C. Reeder, S. Bandyopadhyay, M.L. Klein, J. Phys. Chem. B **105**, 4464 (2001).
9. R. Goetz, G. Gompper, R. Lipowsky, Phys. Rev. Lett. **82**, 221 (1999).
10. J.H. Fendler, *Membrane Mimetic Chemistry* (Wiley, New York, 1982).
11. M.P. Allen, D.J. Tildesley, *Computer Simulations of Liquids* (Oxford University Press, Oxford, 1987).
12. E. Egberts, H.J.C. Berendsen, J. Chem. Phys. **89**, 3718 (1988).
13. M.H. Cohen, D. Turnbull, J. Chem. Phys. **52**, 3038 (1970).
14. M.H. Cohen, G.S. Grest, Adv. Chem. Phys. **48**, 455 (1981).
15. J.D. Ferry, *Viscoelastic Properties of Polymers* (John Wiley and Sons, Inc., 1980).
16. H. Löwen, in *Statistical Physics and Spatial Statistics*, edited by K.R. Mecke, D. Stoyan (Springer, Berlin, 2000).
17. W.L.C. Vaz, R.M. Clegg, D. Hallmann, Biochemistry **24**, 781 (1985).
18. P.F.F. Almeida, W.L.C. Vaz, T.E. Thomson, Biochemistry **31**, 6739 (1992).
19. P.F.F. Almeida, in *Structure and Dynamics of Membranes*, *Handbook of Biological Physics*, Vol. **1**, edited by R. Lipowky, E. Sackmann (Elsevier, Amsterdam, 1995).
20. J.M. Polson, I. Vattulainen, H. Zhu, M.J. Zuckermann, Eur. Phys. J. E **5**, 485 (2001).
21. F. Kamp, D. Zakim, F. Zhang, N. Noy, J.A. Hamilton, Biochemistry **34**, 11928 (1995).
22. A.M. Kleinfeld, J. Membrane Biol. **175**, 79 (2000).